Pergamon

Int. J. Heat Mass Transfer. Vol. 40, No. 15, pp. 3537–3546, 1997

Printed in Great Britain
0017–9310/97 $17.00+0.00

PII: S0017–9310(97)00014–8

A quasi-three-dimensional approach to simulate the two-phase fluid flow and heat transfer in condensers

CHAO ZHANG† and ATISH BOKIL

Department of Mechanical and Materials Engineering, University of Windsor, Windsor, Ontario, Canada N9B 3P4

(*Received* 14 *June* 1996 *and in final form* 20 *December* 1996)

Abstract—A quasi-three-dimensional algorithm is developed to simulate two-phase fluid flow and heat transfer in the shell-side of power plant condensers. The simulation method developed is based on the fundamental governing conservation equations of mass and momentum for both vapor-phase and liquid-phase, and air mass fraction conservation equation. The three-dimensional effects due to the cooling water temperature difference are taken into account by a series of two-dimensional calculations. The numerical predictions of an experimental steam condenser are compared with the experimental results. The predicted results are in good agreement with the experimental data. The predicted results also show an improvement over the results obtained using single-phase model. © 1997 Elsevier Science Ltd.

1. INTRODUCTION

A condenser is an important component that affects the efficiency and performance of power plants. Development of advanced numerical methods for shell-side flows in condensers is a critical step in improving current condenser design techniques. The advantage of numerical simulations is that they can provide a more detailed information on fluid flow and heat transfer in the tube bundle. This information may eliminate, in the early stages of the design process, problems related with flow induced vibration and flow maldistribution, and eventually improve overall heat transfer coefficients and increase the unit performance and reliability. Until now, these simulations have been carried by using either single-phase two-dimensional models [1–3], or single-phase quasi-three-dimensional models [4], or two-phase two-dimensional models [5, 6].

The shell-side flow within large power plant condensers, usually, is three-dimensional. The steam flow in different sections along the cooling water flow direction will differ due to the rise of the cooling water temperature. The quasi-three-dimensional approach takes into consideration the three-dimensional aspects of the flow due to the cooling water temperature difference.

The liquid phase affects the fluid flow and heat transfer in the condenser by virtue of interphase friction force and forming films on the tubes. There is a need to understand the physical behaviour of the condensate, involving its form and its effect, in condensers. In the design of condensers, the assumption is usually made that heat transfer is reduced in the lower tubes of a tube bundle by the increase in film thickness because of condensate raining from the tubes above. This condensate would inundate the steam space producing thicker water coatings on the cooling tubes causing a decrease in the heat transfer. The numerical simulations by using the single-phase model show the region of minimum heat transfer to be present in the lower half of the tube bundle. Recent experimental results [5, 6], however, have shown that the region of minimum heat transfer is in the upper half of the tube bundle.

The purpose of the present work is to develop a numerical simulation model that includes the effects of both three-dimensional and two-phase flow to predict the fluid flow and heat transfer in a condenser more accurately. The flow situation and experimental data of a steam surface condenser are taken from Ref. [5] and Ref. [6]. The numerical results obtained by the proposed numerical model are compared against the experimental data and the predicted results by using the single-phase numerical model.

2. CONDENSER CONFIGURATION

The configuration of the experimental steam surface condenser at NEI Parsons is depicted in Fig. 1. The tube bundle is composed of 20×20 tubes of equilateral triangular arrangement. The cooling water is arranged to flow in a single pass through the condenser. This experimental condenser was designed to demonstrate the effects of air pockets. It is not a good example of condenser design; however, this condenser can be used to test numerical models. The steam enters the con-

† Author to whom correspondence should be addressed.

NOMENCLATURE

A	heat transfer area of a given control volume
A_d	total projected area of droplets in a given control volume
C_f	interphase friction coefficient
c_p	specific heat at constant pressure
c	condensation rate in the control volume under consideration
D	diffusivity of air in steam
D_d	droplet diameter
D_e	effective diffusivity of air in steam $(=D+D_t)$
D_i	inner diameter of the tube
D_o	outer diameter of the tube
D_t	turbulent diffusivity of air in steam
F_u	flow resistance force in the x-momentum equation
F_v	flow resistance force in the y-momentum equation
f	friction factor
Gr	Grashof number
g	gravitational acceleration
H	non-dimensional number of condensation
k	thermal conductivity
L	latent heat of condensation
$\dot{M}$	steam condensation rate
$\dot{m}$	steam condensation rate per unit volume
Nu	Nusselt number
Pr	Prandtl number
P_t	tube pitch
p	pressure
q''	heat flux
Re	Reynolds number
R_a	air resistance
R_c	thermal resistance for condensation heat transfer
R_f	fouling resistance
R_g	volume fraction of vapor-phase
R_l	volume fraction of liquid-phase
R_t	tube wall resistance
R_w	waterside thermal resistance
T	temperature
U_p	velocity magnitude $(=u^2+v^2)^{1/2}$
u	velocity component in the x-direction
V	volume
v	velocity component in the y-direction
w	total amount of condensate leaving the particular control volume
x	steam main flow direction coordinate
y	steam cross flow direction coordinate.

Greek symbols

β	local porosity
β_t	porosity in tube bundle region
μ	laminar dynamic viscosity
μ_e	effective viscosity $(=\mu+\mu_t)$
μ_t	turbulent viscosity
ξ	pressure loss coefficient
ρ	density
ϕ	air mass fraction.

Subscripts

a	air
c	condensate
cs	steam-condensate interface
d	droplet
g	vapor-phase
i	phase in question
l	liquid-phase
s	steam
t	tube
u	parameter in x-momentum equation
v	parameter in y-momentum equation
w	cooling water
x	variable in x-direction
y	variable in y-direction.

denser from the left-hand side. Air and uncondensed steam are extracted to the internal vent as shown in the figure. The condensate is removed from the bottom of the condenser. The geometrical and operating parameters are listed in Table 1. Measurements of mean heat flux were obtained along the third, eighth, 13th, and 18th tube rows from the bottom of the tube bundle [5, 6].

3. NUMERICAL MODEL

In steam condensers, steam and air mixture forms the vapor-phase while the condensed water forms the liquid-phase. The liquid condensate exists as film on the tubes and as droplets or columns between the tubes. Several mechanisms of heat and mass transfer take place between the phases. There is an entrainment of liquid from the films to form droplets. The droplets impinge onto the tubes. Heat transfer from vapor to condensate film takes place due to condensation. Inter-phase friction exists between the vapor and the droplets. Similarly, friction exists between the vapor and the film, and between the film and the tubes. Also, three-dimensional effects occur in condensers primarily due to the cooling water temperature gradients, which lead to space-variable sink potential. The

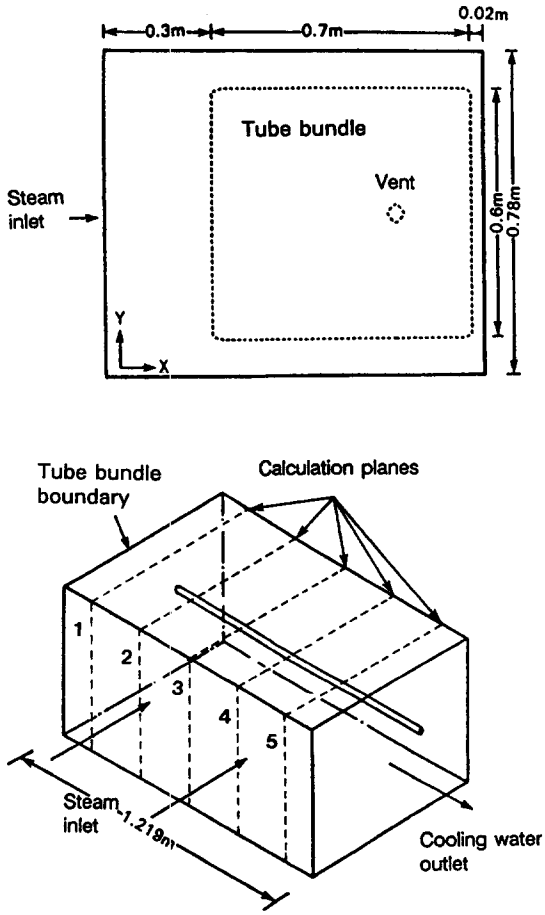

Fig. 1. Configuration of experimental condenser.

Table 1. Geometrical and operating parameters

Geometrical parameters	
Condenser length (m)	1.219
Condenser depth (m)	1.02
Condenser height (m)	0.78
Tube outer diameter (mm)	25.4
Tube wall thickness (mm)	1.25
Tube pitch (mm)	34.9
Operator parameters	
Inlet temp. of cooling water (°C)	17.8
Inlet velocity of cooling water (m s^{-1})	1.19
Inlet pressure of steam (Pa)	27670
Inlet steam flow rate (kg s^{-1})	2.032
Inlet air flow rate (kg s^{-1})	2.48×10^{-4}

fluid flow and heat transfer will differ in the cooling water flow direction.

3.1. *Physical representation*

Usually, the flow behaviour within the tube bundle of a steam condenser is very complicated. Making a number of assumptions is therefore necessary based on the likely characteristics of the flow. In this study, the following major elements are proposed for the complete physical model.

- Mixture of air and steam is considered as a perfect gas, the proportions being defined by the air mass fraction.
- Both steam and liquid condensate are assumed to be saturated.
- Liquid condensate exists as droplets of single size so there will be no diffusion terms for the condensate.
- There is no heat transfer between the steam and the droplets.
- Pressure is assumed common to both phases.
- Mass sink term for vapor associated with condensation is equal to the mass source term for the liquid.
- The turbulent diffusivity is equal to the turbulent viscosity, i.e. Schmidt number is equal to one.
- Pressure drop from inlet to vent for all sectors must be the same.

3.2. *Mathematical formulation*

The simulation method developed in this study is based on the fundamental governing equations of mass, momentum and air mass fraction conservation with flow, heat and mass transfer resistances. Coupled momentum equations for each phase are solved along with the continuity equations to obtain the volume fractions, velocity fields, shared pressure, and air mass fraction. The effect of liquid-phase on the vapor-phase is through the interphase friction. The condenser shell-side is divided into several sectors along the cooling water flow direction and the flow is assumed to be two-dimensional in each sector. The three-dimensional effects due to the cooling water temperature gradients are taken into account by a series of step by step two-dimensional calculations, each being for one sector.

The porous medium concept is used in the simulations. A porosity factor is incorporated into the governing equations to account for the flow volume reduction due to the tube bundles, baffles and other internal obstacles. A pressure correction equation is obtained from the vapor-phase continuity equation and vapor-phase momentum equations. Liquid volume fractions are obtained from the liquid-phase continuity equation. The vapor volume fractions are obtained by using an auxiliary equation.

3.2.1. *Governing equations.* The governing equations are two sets of conservation equations of mass and momentum in each phase, and the conservation equation of air mass fraction. The interphase friction forces used by Bush *et al.* [6] are included in the momentum conservation equations for both vapor-phase and liquid-phase. In the liquid-phase momentum equations, diffusive terms are neglected since the liquid condensate is assumed to exist as droplets of a single size. Then the governing equations become:

Vapor-phase mass conservation equation

$$\frac{\partial}{\partial x}(R_g \rho_g u_g) + \frac{\partial}{\partial y}(R_g \rho_g v_g) = -\dot{m}. \quad (1)$$

Vapor-phase momentum conservation equations

$$\frac{\partial}{\partial x}(R_g\rho_g u_g u_g)+\frac{\partial}{\partial y}(R_g\rho_g v_g u_g)$$
$$=2\frac{\partial}{\partial x}\left(R_g\mu_e\frac{\partial u_g}{\partial x}\right)-\frac{2}{3}\frac{\partial}{\partial x}\left[R_g\mu_e\left(\frac{\partial u_g}{\partial x}+\frac{\partial v_g}{\partial y}\right)\right]$$
$$+\frac{\partial}{\partial y}\left[R_g\mu_e\left(\frac{\partial u_g}{\partial y}+\frac{\partial v_g}{\partial x}\right)\right]-R_g\frac{\partial p}{\partial x}-\dot{m}u_g$$
$$+C_{fu}(u_l-u_g)-R_gF_{ug} \quad (2)$$

$$\frac{\partial}{\partial x}(R_g\rho_g u_g v_g)+\frac{\partial}{\partial y}(R_g\rho_g v_g v_g)$$
$$=\frac{\partial}{\partial x}\left[R_g\mu_e\left(\frac{\partial u_g}{\partial y}+\frac{\partial v_g}{\partial x}\right)\right]+2\frac{\partial}{\partial y}\left(R_g\mu_e\frac{\partial v_g}{\partial y}\right)$$
$$-\frac{2}{3}\frac{\partial}{\partial y}\left[R_g\mu_e\left(\frac{\partial u_g}{\partial x}+\frac{\partial v_g}{\partial y}\right)\right]$$
$$-R_g\frac{\partial p}{\partial y}-\dot{m}v_g+C_{fv}(v_l-v_g)-R_gF_{vg}. \quad (3)$$

Liquid-phase mass conservation equation

$$\frac{\partial}{\partial x}(R_l\rho_l u_l)+\frac{\partial}{\partial y}(R_l\rho_l v_l)=\dot{m}. \quad (4)$$

Liquid-phase momentum conservation equations

$$\frac{\partial}{\partial x}(R_l\rho_l u_l u_l)+\frac{\partial}{\partial y}(R_l\rho_l v_l u_l)$$
$$=-R_l\frac{\partial p}{\partial x}+\dot{m}u_l+C_{fu}(u_g-u_l)-R_lF_{ul} \quad (5)$$

$$\frac{\partial}{\partial x}(R_l\rho_l u_l v_l)+\frac{\partial}{\partial y}(R_l\rho_l v_l v_l)$$
$$=-R_l\frac{\partial p}{\partial y}+\dot{m}v_l+C_{fv}(v_g-v_l)-R_lF_{vl}+R_l\rho_l g. \quad (6)$$

Conservation of air mass fraction

$$\frac{\partial}{\partial x}(R_g\rho_g\phi u_g)+\frac{\partial}{\partial y}(R_g\rho_g\phi v_g)$$
$$=\frac{\partial}{\partial x}\left(R_g\rho_g D_e\frac{\partial\phi}{\partial x}\right)+\frac{\partial}{\partial y}\left(R_g\rho_g D_e\frac{\partial\phi}{\partial y}\right). \quad (7)$$

The dependent variables are velocity components, u_g, v_g, u_l and v_l, pressure, p, liquid volume fraction, R_l, and air mass fraction, ϕ.

3.2.2. *Auxiliary relations.*

3.2.2.1. Volume fractions. The isotropic porosity, β, which is employed to describe the flow volume reduction due to the tube bundles, is defined as the ratio of the volume occupied by the fluid to the total volume. Since the tube bundle is laid out in an equilateral triangular pattern, the porosity in the tube bundle region, β_t, is given as:

$$\beta_t=1-\frac{\pi}{2\sqrt{3}}\left(\frac{D_o}{P_t}\right)^2. \quad (8)$$

In the tube bundle region, $\beta=\beta_t$; in the untubed region, $\beta=1$. The vapor volume fraction and liquid volume fraction are defined as the ratio of the volume occupied by the vapor to the total volume, and the ratio of the volume occupied by the liquid to the total volume, respectively. Thus,

$$R_g+R_l=\beta. \quad (9)$$

3.2.2.2. Momentum source terms. The interphase friction forces in momentum equations are related to the interphase friction coefficient, C_f, which is given as:

$$C_{fu}=\tfrac{1}{2}\rho_g f_d A_d|(u_g-u_l)|$$
$$C_{fv}=\tfrac{1}{2}\rho_g f_d A_d|(v_g-v_l)| \quad (10)$$

where:

$$A_d=\frac{1.5R_lV}{D_d}.$$

Friction factor, f_d, for spherical objects is obtained from an empirical correlation given by Clift *et al.* [7]. The local hydraulic flow resistance forces, F_{ui} and F_{vi}, in the vapor-phase and liquid-phase momentum equations due to the tube bundle are given as:

$$F_{ui}=\xi_{ui}\rho_i u_i U_{pi}$$
$$F_{vi}=\xi_{vi}\rho_i v_i U_{pi} \quad (11)$$

where ξ_{ui} and ξ_{vi} are the pressure loss coefficients. The expressions proposed by Rhodes and Carlucci [8] for the loss coefficients are used, namely:

$$\xi_u=2\left(\frac{f_u}{P_t}\right)\left(\frac{P_t\beta}{P_t-D_o}\right)^2\left(\frac{1-\beta}{1-\beta_t}\right)$$
$$\xi_v=2\left(\frac{f_v}{P_t}\right)\left(\frac{P_t\beta}{P_t-D_o}\right)^2\left(\frac{1-\beta}{1-\beta_t}\right) \quad (12)$$

where

$$f_u=\begin{cases}0.619Re_u^{-0.198}; & Re_u<8000\\ 1.156Re_u^{-0.2647}; & 8000\leqslant Re_u<2\times10^5\end{cases}$$

$$f_v=\begin{cases}0.619Re_v^{-0.198}; & Re_v<8000\\ 1.156Re_v^{-0.2647}; & 8000\leqslant Re_v<2\times10^5.\end{cases}$$

3.2.2.3. Mass source term. The mass source term, $\dot{m}$, is the steam mass condensation rate per unit volume. The condensation takes place only on the cooling tubes since no condensation or re-evaporation from the condensate droplets is assumed. The steam mass condensation rate per unit volume can be calculated by equating the phase change enthalpy with the heat transfer rate from the steam to the cooling water flowing in the tubes, as follows:

$$\dot{m}LV = \frac{T - T_w}{R} A. \quad (13)$$

The cooling water temperature, T_w, is obtained by the heat balance between the steam and the cooling water in each control volume. The overall thermal resistance for each control volume, R, is the sum of all individual resistances calculated from various semi-empirical heat transfer correlations,

$$R = R_w \frac{D_o}{D_i} + R_t + R_c + R_a. \quad (14)$$

For the waterside thermal resistance, R_w, the relationship given by Ditus and Boelter [9] can be employed,

$$\frac{1}{R_w} = 0.023 \frac{k_w}{D_i} Re_w^{0.8} Pr_w^{0.4}. \quad (15)$$

The tube wall resistance, R_t, is calculated from the following expression:

$$R_t = \frac{D_o \ln(D_o/D_i)}{2k_t}. \quad (16)$$

The thermal resistance for condensation heat transfer, R_c, is determined by using modified Nusselt's correlation [10–12].

$$\frac{1}{R_c} = Nu \frac{k}{D_o} [1 + 0.0095(Re_s)^{11.8/\sqrt{Nu}}] \left(\frac{w}{c}\right)^{-0.16} \quad (17)$$

where:

$$Nu = 0.725 \left(\frac{Gr}{H}\right)^{1/4}; \quad Gr = \left(\frac{D_0^3 g}{\mu_c^2}\right)[\rho_c(\rho_c - \rho_s)]$$

$$H = \frac{c_{pc}(T_s - T_w)}{Pr_c L}; \quad Re_s = \frac{\rho_s U_p D_0}{\mu_s}.$$

The resistance from the presence of air film is evaluated via a mass transfer coefficients as reported by Berman and Fuks [13].

$$\frac{1}{R_a} = a \frac{D}{D_o} Re_s^{1/2} \left(\frac{p}{p - p_s}\right)^b p^{1/3} \left(\rho_s \frac{L}{T}\right)^{2/3} \frac{1}{(T - T_{cs})^{1/3}} \quad (18)$$

where:

$$a = 0.52, b = 0.7 \quad \text{for } Re_s < 350;$$

$$a = 0.82, b = 0.6 \quad \text{for } Re_s > 350.$$

3.2.2.4. Other properties. The density of the mixture varies locally according to the perfect gas equation of state. Turbulent viscosity, μ_t, is taken as a constant (forty times the value of the dynamic viscosity) throughout. The droplet diameter is set to equal 1 mm as suggested by Al-Sanea *et al.* [5].

3.3. *Numerical solution*

The discretization of the differential equations, equations (1)–(7), is carried out by integrating them over small control volumes in a staggered grid. The resulting discretized equations are solved in primitive variables. These equations are coupled and are highly nonlinear. Thus, an iterative approach is used for their solution.

The condenser is divided into five sectors normal to the cooling water flow direction as shown in Fig. 1. The sectors interact with each other through the 'thermal memory' of the cooling water on the tube side. Calculations are performed for each plane, which is located at the middle of the sector and normal to the cooling water flow direction, sequentially starting from the cooling water inlet end. The outlet cooling water temperature for the preceding sector is taken as the inlet cooling water temperature for the following sector. Thus, the three-dimensional effects due to the cooling water temperature difference are propagated from one sector to the other. The inlet mass flow rate for each sector is used to calculate the inlet mixture velocity, which is the inlet boundary condition for the calculation. The inlet mass flow rate into each sector is determined by the constraint that the pressure drop from inlet to the vent for all the sectors must be identical since the sectors share the same inlet and vent. This is called pressure drop balance [14]. To satisfy this constraint, repeated amendments are made for the inlet mass flow rate to each sector. Figure 2 shows the flow chart of the proposed numerical procedure. The grid-independent test indicated that a grid of 31×34 in the x and y directions respectively will give essentially grid-independent results [4]. Thus, a grid of 31×34 is employed in the calculations as shown in Fig. 3.

4. RESULTS

4.1. *Typical results*

Figure 4 shows the vapor-phase velocity vector plot. It can be noticed that some deflection of the flow occurs away from the tube bundle due to the flow resistance from the presence of tubes. On the rear end of the condenser, the flow turns towards the tube bundle due to the rear wall and the suction caused by the condensation in the tube bundle. The vapor velocity, inside the tube bundle, continues reducing as the steam condenses and becomes very small in the central region of the tube bundle. An increase in the vapor velocity at the entrance to the tube bundle is attributed to the sudden decrease in the flow area due to the presence of the tubes. The liquid velocities appear only after the steam–air mixture enters the tubular region and starts condensing as shown in Fig. 5. The x-direction velocity components are dominant at the inlet of and the bottom of the tube bundle, while gravity clearly dominates elsewhere in the tubular region and the condensate falls nearly vertically. Though the condensate falls under the influence of gravity, it is also subjected to interphase frictional forces which deflect its course.

The contour maps for vapor-phase and liquid-phase

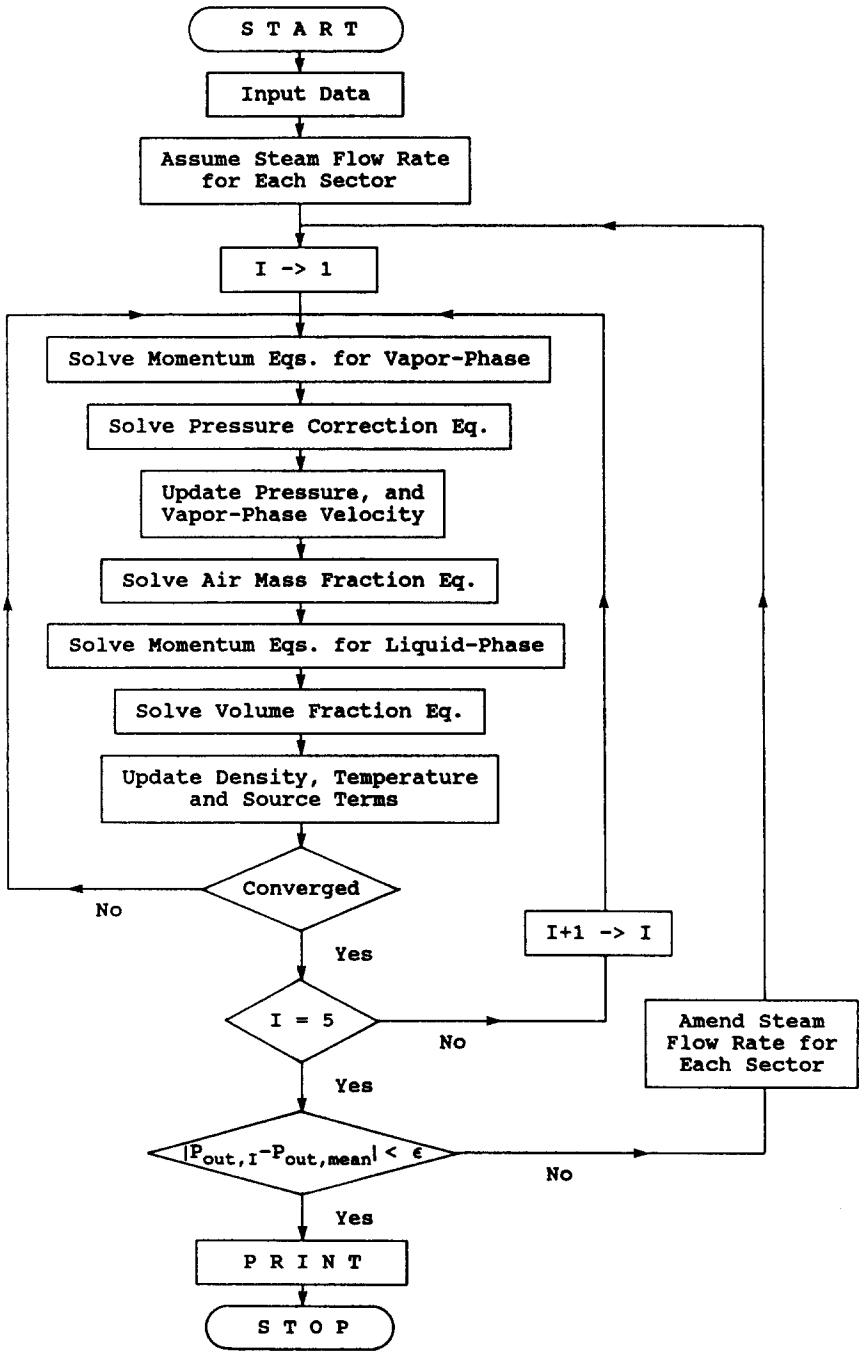

Fig. 2. Flow chart.

velocity magnitudes are shown in Figs. 6 and 7, respectively. In the vapor velocity contour, the increase in the velocity at the entrance to the tube bundle can be clearly seen. In the liquid-phase velocity contour, higher velocities are observed in the region just below the tube bundle and the region near the rear wall due to the high vapor velocity in these regions which forces the liquid along with it.

Figure 8 depicts the steam condensation rate along the tube axial direction. The results can be explained by considering the three-dimensionality of the steam flow in the condenser. Due to the varying cooling water temperature along the condenser, as expected, the condensation rate is greater at the cooling water inlet end than that at the outlet end.

The contours of heat flux distributions at the first and the last planes are shown in Fig. 9. The distributions of the heat flux at the second, third, and fourth planes which are not shown in the figure have the patterns similar to these at the first and the last planes. Corresponding with the lower vapor velocity region is the region of lower heat transfer. The highest

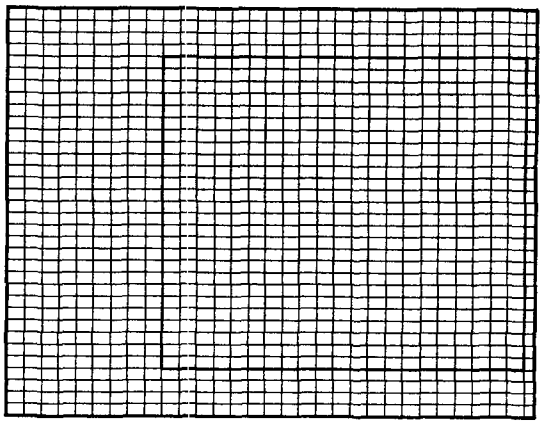

Fig. 3. Grid used for the simulation.

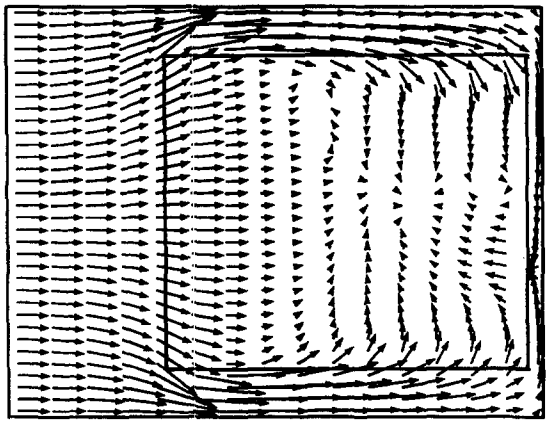

Fig. 4. Vapor-phase velocity vector plot for plane no. 1.

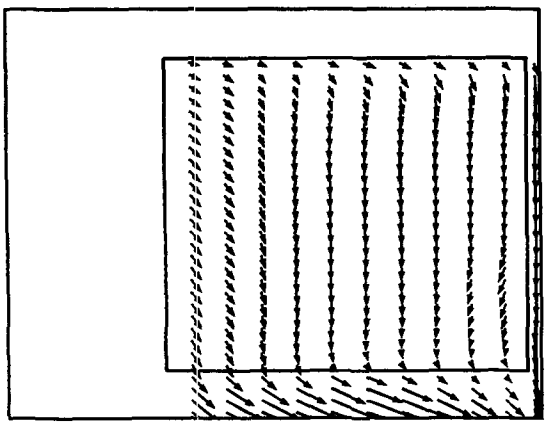

Fig. 5. Liquid-phase velocity vector plot for plane no. 1.

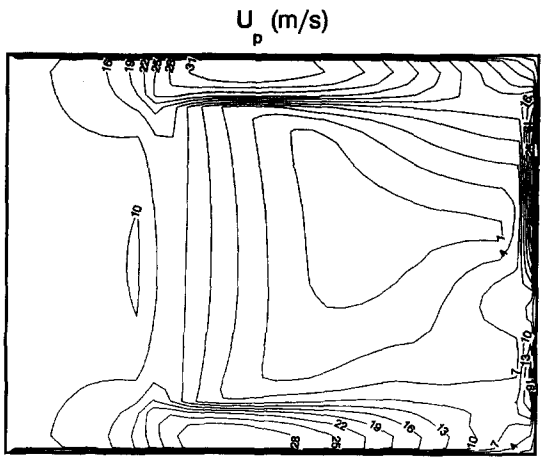

Fig. 6. Contour map of vapor velocity magnitude for plane no. 1.

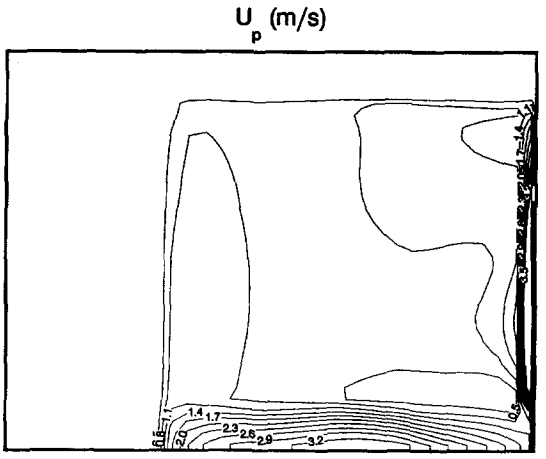

Fig. 7. Contour map of liquid velocity magnitude for plane no. 1.

heat flux is at the entry to the tube bundle, where steam velocities are the highest and air concentration is the lowest. The heat flux is high at the periphery of the tube bundle and falls to a low value in the vent area. Contrary to the widely held view of a reduction in heat transfer in the lower region of a condenser tube bundle due to the inundation effect, the lower heat transfer zone is in the upper tubular region. One possible explanation is that the turbulence of the condensate film on the lower tubes in the tube bundle is strongly enhanced due to splashing of condensate droplets from above. On comparing the heat flux in different planes, it can be seen that there is a decrease in the average heat flux from the first plane to the last plane. This reflects the influence of the three-dimensionality of the flow, which agrees with the steam condensation rate distribution.

The liquid volume fraction contour is shown in Fig. 10. The liquid volume fraction is the highest in the lower part of the tubular region since the amount of liquid is higher there.

4.2. *Comparison with experimental data*

Comparisons between the predictions obtained by the proposed quasi-three-dimensional, two-phase numerical model and the measurements are made for heat flux distributions. Figures 11–14 show the comparison of the heat flux along four of the tube rows with the experimental data. Since the experimental heat flux at each plane is not available and the experimental values are mean values along the cooling water flow direction, the predicted data used here are

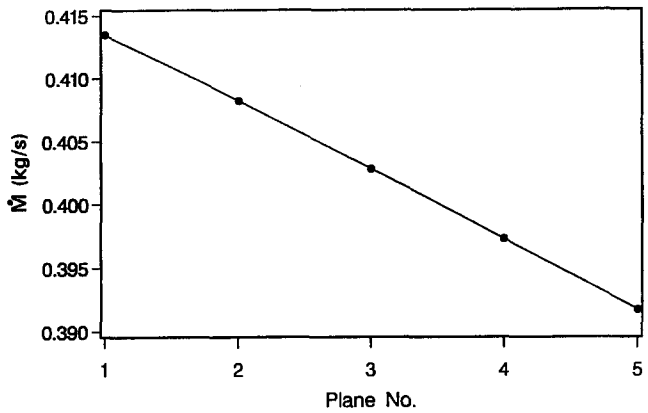

Fig. 8. Distribution of condensation rate.

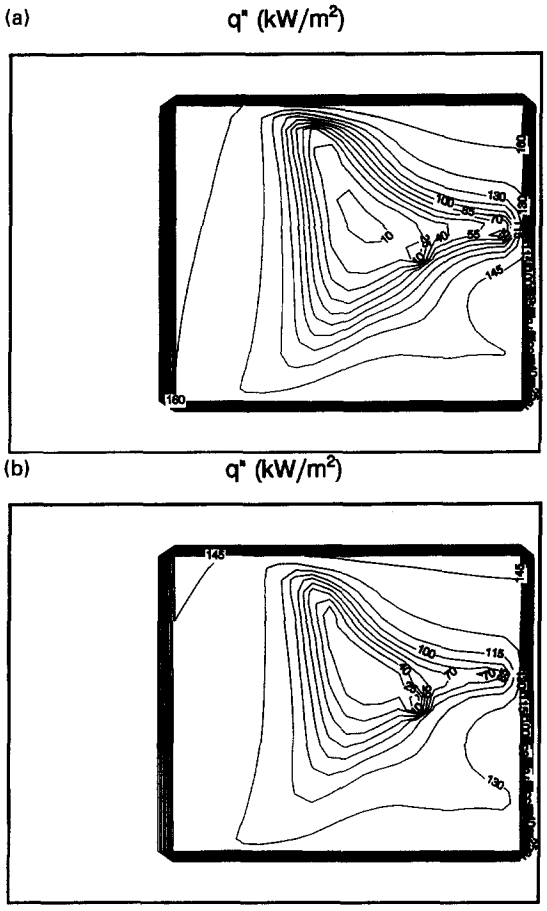

Fig. 9. Contour map of heat flux. (a) Plane no. 1; (b) plane no. 5.

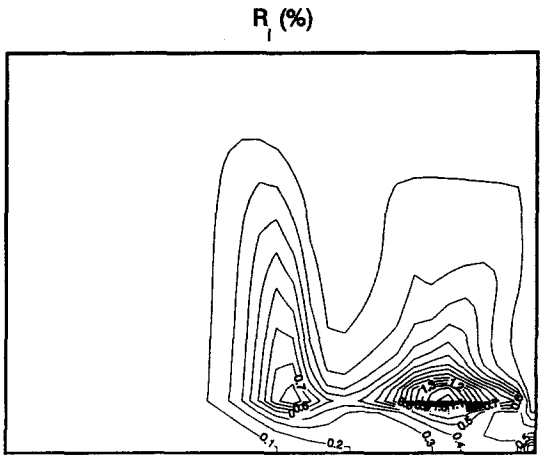

Fig. 10. Contour map of liquid volume fraction for plane no. 1.

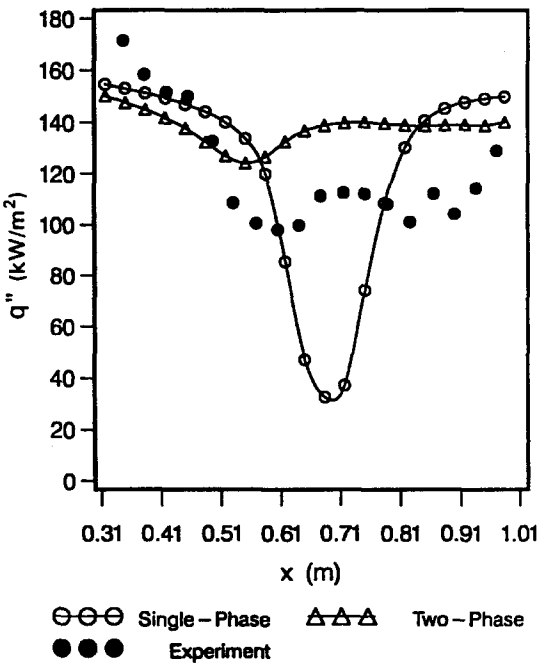

Fig. 11. Heat flux along the third row from the bottom of the tube bundle.

average values of these from the five sectors. The values of heat fluxes along all the four tube rows show that the variation is similar to that in the experimental case. The agreement with experiment results is good for the upper three tube rows. There is some over prediction of heat flux for the bottommost tube row. It is noted from the predicted results that the regions of minimum heat transfer are in the upper half of the tube bundle, i.e. along the 13th and 18th tube rows

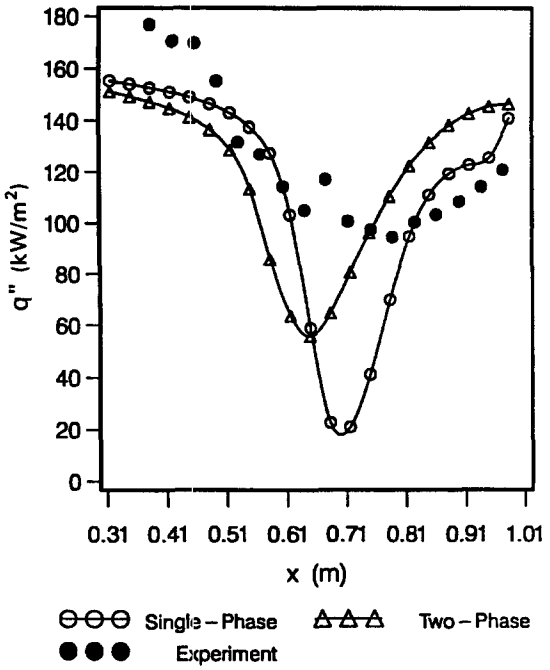

Fig. 12. Heat flux along the eighth row from the bottom of the tube bundle.

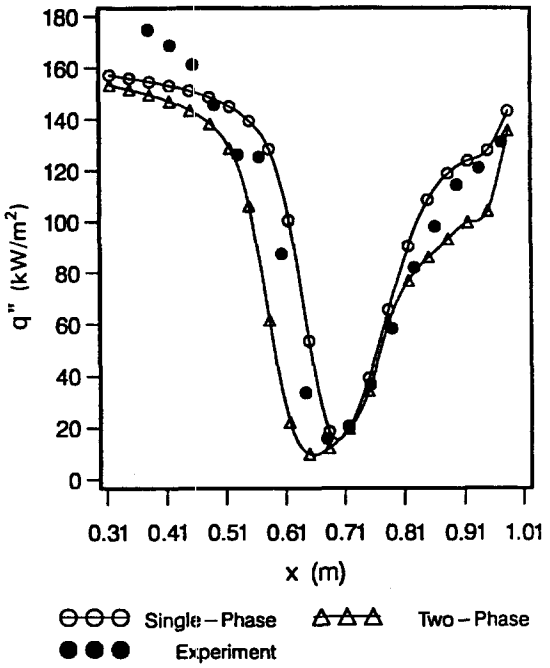

Fig. 13. Heat flux along the 13th row from the bottom of the tube bundle.

from the bottom of the tube bundle, as shown in the figures. This agrees with the experimental data.

The predicted total condensation rate (2.014 kg s^{-1}) is in excellent agreement with the experimental value (2.021 kg s^{-1}).

The predicted results using the proposed numerical model are also compared with the results obtained by using the quasi-three-dimensional single-phase

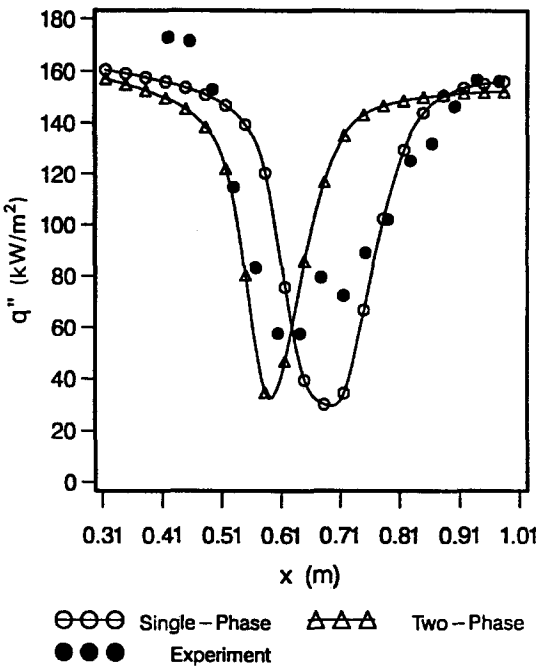

Fig. 14. Heat flux along the 18th row from the bottom of the tube bundle.

numerical model [4] as shown in Figs. 11–14. As it can be seen from these figures, there is a good agreement between the experiments and the predictions using both single-phase and two-phase models in the upper half of the condenser (13th and 18th tube rows from the bottom). The reason is that the effect of the liquid-phase is not significant in the upper tube bundle. However, for the lower half the tube bundle (third and eighth tube rows from the bottom), the heat fluxes obtained by the single-phase model are under-predicted in the central part of the tubular region. The liquid has strong influence in the lower part of the tubular region because most of the condensate accumulates there. In the single-phase model, the effect of liquid droplets is not taken into consideration. This is probably the reason for discrepancies in the single-phase model results.

5. CONCLUSION

A quasi-three-dimensional two-phase numerical model to predict the fluid flow and heat transfer in condensers has been developed. The simulations have been carried out for an experimental condenser. The numerical model has successfully reproduced the main features of the flow inside the stream condenser. the numerical model proposed in the present study has shown the capability of predicting the performance of condensers. The agreement with the experimental results is good in most regions of the tube bundle. On comparing the results from the quasi-three-dimensional two-phase model with those from the quasi-three-dimensional single-phase model, it has been seen that the quasi-three-dimensional two-phase model

gives better results in the lower part of the tubular region where the liquid plays a major role. In the upper part of the tubular region, results from the two-phase model are similar to those from the single-phase model.

Acknowledgement—Financial support for this work was received from the University of Windsor and Natural Sciences and Engineering Research Council of Canada (NSERC Grant no. OGP-0105727).

REFERENCES

1. Davidson, B. J. and Rowe, M., Simulation of power condenser performance by computation method: an overview. In *Power Condenser Heat Transfer Technology*, ed. P. Marto and R. Nunn. Hemisphere, Washington, 1981, pp. 17–49.
2. Caremoli, C., Numerical computation of steam flows in power plant condensers. In *Numerical Methods in Thermal Problems*, ed. R. W. Lewis and K. Morgan. Pineridge Press, Swansea, U.K., 1985, pp. 315–325.
3. Al-Sanea, S., Rhodes, N., Tatchell, D. G. and Wilkinson, T. S., A computer model for detailed calculation of the flow in power station condensers. *Condenser: Theory and Practice*, In *International Chemical Engineering Symposium Series*, no. 75. Pergamon Press, Oxford, 1983, pp. 70–88.
4. Zhang, C. and Zhang, Y., A quasi-three-dimensional approach to predict the performance of steam surface condensers. *Journal of Energy Resources Technology*, 1993, **115**(3), 213–220.
5. Al-Sanea, S., Rhodes, N. and Wilkinson, T. S., Mathematical modelling of two-phase condenser flows. In *Proceedings of the International Conference on Multiphase Flow*, London, 1985, pp. 19–21.
6. Bush, A. W., Marshall, G. S. and Wilkinson, T. S., A prediction of steam condensation using a three component solution algorithm. In *Proceedings of The Second International Symposium on Condensers and Condensation*, University of Bath, U.K., 1990, pp. 223–234.
7. Clift, R., Grace, J. R. and Weber, M. E., *Bubbles, Drops and Particles*. Academic Press, New York, 1978.
8. Rhodes, D. B. and Carlucci, L. N., Predicted and measured velocity distributions in a model heat exchanger. In *International Conference on Numerical Methods in Nuclear Engineering*. Canadian Nuclear Society–American Nuclear Society, Montreal, 1983.
9. Ditus, F. W. and Boelter, L. M. K., Heat transfer in automobile radiators of the tubular type. *University of California at Berkeley, Publications in Engineering*, 1930, **2**, 443–461.
10. Grant, I. D. R. and Osment, B. D. J., The effect of condensate drainage on condenser performance. NEL Report No. 350, April, 1968.
11. Fuks, S. N., Heat transfer with condensation of steam flowing in a horizontal tube bundle. *Teploenergetika*, 1957, **4**, 35–39.
12. Wilson, J. L., The design of condensers by digital computers. *International Chemical Engineering Symposium Series*, 1972, **35**, 132–151.
13. Berman, L. D. and Fuks, S. N., Mass transfer in condensers with horizontal tube when the steam contains air. *Teploenergetika*, 1958, **5**(8), 66–74.
14. Barsness, E. J., Calculation of the performance of surface condenser by digital computer. In *National Power Conference*, Cincinnati, Ohio. ASME Paper, no. 63-PWR-2, 1963.